Electrolyte Screening Effect on the Photoprotolytic Cycle of Excited Photoacid in Ice

Anna Uritski, Pavel Leiderman, and Dan Huppert*

Raymond and Beverly Sackler Faculty of Exact Sciences, School of Chemistry, Tel Aviv University, Tel Aviv 69978, Israel

Received: September 19, 2006; In Final Form: October 23, 2006

Time-resolved emission was used to measure the photoprotolytic cycle of an excited photoacid as a function of temperature, both in liquid water and in ice, in the presence of an inert salt. The inert salt affects the geminate recombination between the transferred proton with the conjugate base of the photoacid. We used the Debye−Hückel theory to express the screening of the Coulomb electrical potential by the inert salt. We find that in the liquid phase the measured screening effect is small and the Debye−Hückel expression slightly overestimates the experimental effect. In ice, the screening effect is rather large and the Debye−Hückel expression under estimates the measured effect. We explain the large screening in ice by the "salting-out" effect in ice that tends to concentrate the impurities to confined volumes to minimize the ice crystal energy.

Introduction

Proton-transfer reactions in solution are common in chemical and biological processes.[1−4] Over the last two decades, intermolecular proton transfer in the excited state (ESPT) has been studied extensively in the liquid phase and provided pertinent information about the mechanism and the parameters controlling acid−base reactions.[5−12] The study of proton reaction in the solid phase and particularly in ice is rare and uncommon.[13,14] In the past the physics of ice[15−18] was studied extensively. Electrical conductivity measurements of Eigen[4] in the early sixties gave a surprising large mobility for the proton in ice. It was estimated[4] that the proton mobility is 10−100 times larger than in water. In numerous further measurements it was found that at about 263 K the proton mobility in ice is smaller by about a factor of 2 than the value of water.[19]

To initiate proton reactions in the liquid and solid phases, protic solvent solutions of photoacids are irradiated by short (femtosecond−picosecond) laser pulses.[20−22] Consequently, the excited-state molecules dissociate very rapidly by transferring a proton to a nearby solvent molecule. The excited-state deprotonated form RO^-* is negatively charged. Thus, the reversible geminate recombination process is strongly enhanced. The proton-transfer rate could be determined either by the initial decay time of the time-resolved fluorescence of the protonated form (ROH*) or by the slow rise time of the emission of the deprotonated species (RO^-*).

Over the past decade we used a model for an intermolecular ESPT process that accounts for the geminate recombination (GR) of the transferred proton. We describe briefly the GR model in a separate subsection.

8-Hydroxypyrene-1,3,6-trisulfonate (HPTS or pyranine) is a photoacid commonly used in the study of ESPT process.[22−25] In previous works[26,27] we presented a comprehensive analysis of salt effects on excited-state intermolecular proton transfer to a liquid solvent from an excited photoacid ROH molecule (HPTS). The dynamics, obtained from the time-resolved fluorescence, were fitted to the geminate recombination model. A large fraction of the time-resolved emission signal of the ROH signal is carried by the long-time fluorescence tail, reflecting the proton−RO^- geminate recombination events.

Proton diffusion, as monitored by photoacid time-resolved fluorescence, is a microscopic process in which the proton surveys the immediate surrounding of the HPTS anion, RO^-*. The time-resolved emission signal contains information on the proton−anion interaction potential and the microscopic proton mobility. The addition of inert salts modifies both attributes. The main effect of added salt is a reduction in the long-time fluorescence tail due to screening of the RO^-−proton Coulomb attraction. In the analysis, it was also found that inert salt also reduces the proton mobility.

In other previous works[28,29] we extended the liquid-phase studies on the protophotolytic cycle of photoacid to the ice phase. The temperature dependence of the excited-state proton-transfer rate in the liquid phase of mild and strong photoacids is rather small. At the high-temperature range $T > 280$ K we found for HPTS that the activation energy E_a is less than 5 kJ/mol. At lower temperatures down to the supercooled region $260 < T < 280$ K, the activation energy is not constant and increases as the temperature decreases. At about 260 K, $E_a \sim 20$ kJ/mol. In ice, in the temperature range $230 < T < 270$ K, we found for the HPTS photoacid a constant activation energy of about $E_a \sim 30$ kJ/mol. In a recent work we extended the previous studies on ESPT in ice and measured the ESPT cycle of HPTS in water containing large concentrations of several electrolytes as well as in frozen water−methanol mixtures.[28] The Arrhenius plot of $\ln(k_{PT})$ versus $1/T$ is nearly constant and the activation energy of the proton transfer of an electrolyte solution is large, twice that in pure water, $E_a \sim 60$ kJ/mol, whereas the activation energy of the proton-transfer rate in the solid phase of the water−methanol mixtures is somewhat lower than in pure water, $E_a \sim 28$ kJ/mol. Careful examination of the time-resolved emission in ice samples shows that the fit quality at low temperatures $T < 240$ K, using the geminate recombination model, is rather poor at short times. We were able to get a better fit using an inhomogeneous kinetics model assuming the proton-transfer rate consists of a distribution of rates. The model is

* Corresponding author. E-mail: huppert@tulip.tau.ac.il. Phone: 972-3-6407012. Fax: 972-3-6407491.

10.1021/jp066127d CCC: $33.50 © 2006 American Chemical Society
Published on Web 12/08/2006

consistent with an inhomogeneous frozen water distribution next to the photoacid.

In this contribution we extend our previous study on electrolyte screening[27] measured at room temperature in the liquid water phase by extending it to the solid ice phase. The Coulomb potential between H^+-RO^- that enhances the geminate recombination is partially screened by immobile inert salt ions in the ice phase. We used two photoacids, HPTS and 2-naphthol-6,8-disulfonate (2N68DS) and two inert salts, $NaNO_3$ and NaCl. 2N68DS (pK^* $\sim$ 0.7) is a stronger photoacid than HPTS (pK^* $\sim$ 1.35). In general, both photoacid results provide the same information on the effective screening of electrolytes in ice. The main finding in the current study is that the screening salt effect in ice is much larger than in the liquid state. We explain the large effect by effective large salt concentration surrounding the photoacid in ice.

Experimental Section

Time-resolved fluorescence was acquired using the time-correlated single-photon counting (TCSPC) technique, the method of choice when sensitivity, a large dynamic range and low-intensity illumination are important criteria in fluorescence decay measurements.

For excitation, we used a cavity dumped Ti:sapphire femtosecond laser, Mira, Coherent, which provides short, 80 fs, pulses of variable repetition rate, operating at the SHG frequency, over the spectral range 380−400 nm with the relatively low repetition rate of 500 kHz. The TCSPC detection system is based on a Hamamatsu 3809U, photomultiplier and Edinburgh Instruments TCC 900 computer module for TCSPC. The overall instrumental response was about 35 ps (fwhm). Measurements were taken at 10 nm spectral width. The observed transient fluorescence signal, $I(t)$, is a convolution of the instrument response function (IRF), $I_0(t)$, with the theoretical decay function. The excitation pulse energy was reduced by neutral density filters to about 10 pJ. We checked the sample's absorption prior to and after time-resolved measurements. We could not find noticeable changes in the absorption spectra due to sample irradiation.

Steady-state fluorescence spectra were taken using a FluoroMax (Jobin Yvon) spectrofluorometer and a miniature CCD spectrograph CVI MS-240. The HPTS, of laser grade, and 2-naphthol-6,8-disulfonate (2N68DS) were purchased from Kodak. Perchloric acid, 70% reagent grade was purchased from Aldrich. For steady-state fluorescence measurements we used photoacid solutions of $\sim 2 \times 10^{-5}$ M. For transient measurements the sample concentrations were between 2×10^{-4} and 2×10^{-5} M. Deionized water had resistance >10 MΩ. methanol, NaCl and $NaNO_3$ of analytical grade, was from Fluka. All chemicals were used without further purification. The solution pH was about 6.

The HPTS fluorescence spectrum at room temperature consists of two structureless broad bands ($\sim$40 nm fwhm). At temperatures below $T < 150$ K the ROH emission band exhibits a distinctive vibration structure. The emission band maximum of the acidic form (ROH*) and the alkaline form (RO^-*) in water are at 445 and 510 nm, respectively. At 435 nm, the overlap of the two luminescence bands is rather small. The contribution of the RO^-* band to the total intensity at 435 nm is less than 0.2%. To avoid overlap between contributions of the two species, we mainly monitored the ROH* fluorescence at 435 nm.

The 2N68DS fluorescence spectrum consists of two structureless broad bands ($\sim$40 nm fwhm). The emission band maximum of the acidic form (ROH*) and the alkaline form (RO^-*) in water are at 370 and 470 nm, respectively. At 370 nm, the overlap of the two luminescence bands is rather small. To avoid overlap between contributions of the two species, we mainly monitored the ROH* fluorescence at 375 nm.

The temperature of the irradiated sample was controlled by placing the sample in a liquid N_2 cryostat with a thermal stability of approximately $\pm$1.5 K.

In the solid phase, the photoacid tends to "salt out" the HPTS and, as a consequence, the luminescence intensity in frozen samples is strongly reduced. The net result is an unreliable time-resolved emission measurements in the ice phase, of both the acid (ROH*) and base (RO^-*) forms. The "salting out" problem of HPTS out of the ice phase was unnoticed when a small amount of methanol, $\sim$1% mole fraction, was added to the solution.

Ice samples were prepared by first placing the cryogenic sample cell, for about 20 min, at a temperature of about 273 K. The second step involved a relatively rapid cooling (10 min) to a temperature of about 250 K. The sample subsequently freezes within 5 min. To ensure ice equilibration prior to the time-resolved measurements, the sample temperature is kept constant at about 250 K for another 30 min.

Reversible Diffusion-Influenced Two-Step Proton-Transfer Model with Inclusion of a Proton Scavenger in Solution

In this model,[12,23,24] the overall dissociation process can be subdivided into the two consecutive steps of reaction and diffusion. In the reactive stage, a rapid short-range charge separation occurs and a solvent-stabilized ion pair is formed. This is followed by a diffusive stage, when the two ions withdraw from each other due to their thermal random motion. The reverse process is a geminate recombination (neutralization) of the two separated ions either by the direct collapse of the ion pair or after a geminate reencounter of the solvated "free" ions.

Mathematically, one considers the probability density, $p(r,t)$, for the RO^-*-H^+ pair to separate to a distance r by time t after excitation. The observed (normalized) signals from the excited acid ROH* and the RO^- anion correspond to the probability, to find the ROH* form $P(t)$, and the survival probability of the separated pair, $S(t)$ which is also the probability to find the excited photoacid in its RO^- form

$$S(t) \equiv 4\pi \int_a^\infty p(r,t) r^2 \, dr \tag{1a}$$

$$P(t) = 1 - S(t) \tag{1b}$$

The separated pair at time t, $p(r,t)$ is assumed to obey a spherically symmetric Debye−Smoluchowski equation (DSE) in three dimensions (2a), which is coupled to a kinetic equation for $P(t)$ (2b), which serves as the boundary condition for the differential equation (2a).[12]

$$\frac{\partial p(r,t)}{\partial t} = \left[r^{-2} \frac{\partial}{\partial r} D r^2 e^{-V(r)} \frac{\partial}{\partial r} e^{V(r)} - k_0' \right] p(r,t) + [k_{PT} P(t) - k_r p(r,t)] \frac{\delta(r-a)}{4\pi a^2} \tag{2a}$$

$$\frac{\partial}{\partial t} P(t) = k_r p(a,t) - (k_{PT} + k_0) P(t) \tag{2b}$$

The geminate recombination is given by a delta function "sink term", $k_r\delta(r - a)/(4\pi a^2)$. In contrast, the ROH* and RO^-* radiative decay rate constants (k_0 and k_0', respectively) are r-independent. The radiative rate of ROH* is determined in the absence of an excited-state proton-transfer reaction (measured in neat methanol solution). When the proton reaches the reaction sphere at $r = a$, it recombines geminately to form back ROH* with a rate constant k_r (reflective boundary condition). The mutual attraction of the proton and the HPTS anion is described by a distance dependent potential, $V(r)$, in units of the thermal energy k_BT. In this study, the ESPT process is examined in the presence of NaCl or $NaNO_3$ salt concentration in an aqueous liquid solution and in ice. To account for the salt effect, we apply the screened Coulomb potential of Debye and Hückel[30]

$$V(r) = -\frac{R_D}{r}\frac{\exp[-\kappa_{DH}(r-a)]}{1+\kappa_{DH}a} \tag{3}$$

where R_D and κ_{DH}^{-1} are the Debye and ionic-atmosphere radii, respectively, and a is its ionic radius.

$$R_D \equiv \frac{|z_1 z_2|e^2}{\epsilon k_B T}$$

$$\kappa_{DH}^{\ 2} \equiv \frac{8\pi e^2 c}{\epsilon_s k_B T}$$

$$\kappa_{DH} \equiv B\sqrt{c} \tag{4}$$

$z_l = 1$, $z_2 = -4$ are the charges of the proton and deprotonated HPTS, respectively (for 2N68DS z_2 equals -3). e is the electronic charge, ϵ_s is the static dielectric constant of the solvent, k_B is Boltzmann's constant, T is the absolute temperature and c is the concentration of the 1:1 electrolyte.

We used the screened Coulomb potential given in eq 3 with the appropriate charges z_l and z_2 (eq 4). The electrolyte screening length κ_{DH} is calculated using eq 4. For water at 298 K, $B = 0.324$ Å^{-1} mol$^{-1/2}$. For the calculation of κ_{DH} in ice we used a temperature-dependent value for the dielectric constant that assumes a value of $\epsilon_s \approx 100$ at about the freezing point. It increases linearly as the temperature decreases.

The relative diffusion constant, D in liquid solution is the sum of the protic and anionic diffusion coefficients. Because the proton is abnormally fast, whereas the anion is bulky and slow, its diffusion coefficient may be neglected with respect to that of the proton. In ice only the proton is mobile and the photoacid and the salt ions are immobile.

As compared with traditional treatments of diffusion-influenced reactions,[31] the new aspect is the reversibility of the reaction, described by the "back-reaction" boundary condition.[24,27,32] The process we wish to consider begins upon photochemical excitation, which prepares an equilibrated thermal and vibronic states of the ROH* acidic form in the lowest electronic state, S_1. Thus, the initial condition is

$$P(0) = 1 \qquad p(r,0) = 0 \tag{5}$$

where $P(0)$ denotes the excited-state ROH probability at $t = 0$.

The bound and dissociated states evolve according to eq 2a with boundary condition set by eq 2b. We solve these equations numerically using the Windows application[33] for solving the spherically symmetric diffusion problem (SSDP), convolute $P(t)$ with the IRF and compare it with the ROH* fluorescence signal.

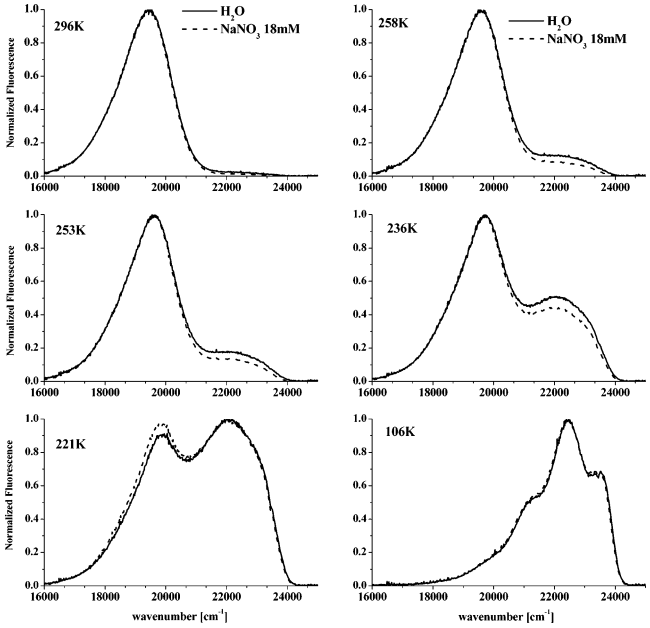

Figure 1. Steady-state emission spectra of an aqueous solution of HPTS and aqueous solution of HPTS containing 18 mM $NaNO_3$ at various temperatures.

The asymptotic expression (the long-time behavior) for the fluorescence of ROH* in the case where both forms of the photoacid, ROH and RO^-, have the same lifetime is given by[27]

$$[\mathrm{ROH}^*]\exp[t/\tau_f] \cong \frac{\pi}{2}a^2(\exp[V(a)])\frac{k_r}{k_{PT}(\pi D)^{3/2}}t^{-d/2} \tag{6}$$

where τ_f is the excited-state lifetime of both the protonated form, ROH, and the deprotonated form, RO^-. d is the dimensionality of the relevant problem, a is the contact radius and k_{PT} and k_r are the proton-transfer and recombination rate constants, respectively. All other symbols are as previously defined. Equation 6 shows that the tail amplitude depends on several parameters but its time dependence is a power law of time that depends on the dimensionality of the problem. For 3 dimensions, it assumes the power law of $t^{-3/2}$.

The absolute fluorescence quantum yield of ROH is given by

$$\Phi(\mathrm{ROH}^*) = \tau_f^{-1}\int_0^\infty P(t)\exp(-t/\tau_f)\,dt \tag{7}$$

Results

Figure 1 shows the steady-state emission spectra of an aqueous solution of HPTS and aqueous solution of HPTS containing 18 mM $NaNO_3$ at various temperatures in the range 100−297 K. Both samples were excited by a short laser pulse at a repetition rate of 500 kHz and the excitation wavelength was at about 400 nm, near the peak absorption of $S_0 \rightarrow S_1$-transition of HPTS in aqueous solution. As seen in the figure, the ROH band maximum is at about 450 nm and the RO^- band maximum at room temperature at about 512 nm. In general, the ROH band intensity is small at room temperature and its amplitude increases as the temperature decreases. At a certain temperature, the two sets of spectra, the one of HPTS in aqueous solution and the solution with a small concentration of an inert salt, are similar in their relative RO^-/ROH intensities.

The increase of the ROH intensity as the temperature decreases is as a result of decrease in the rate of proton transfer

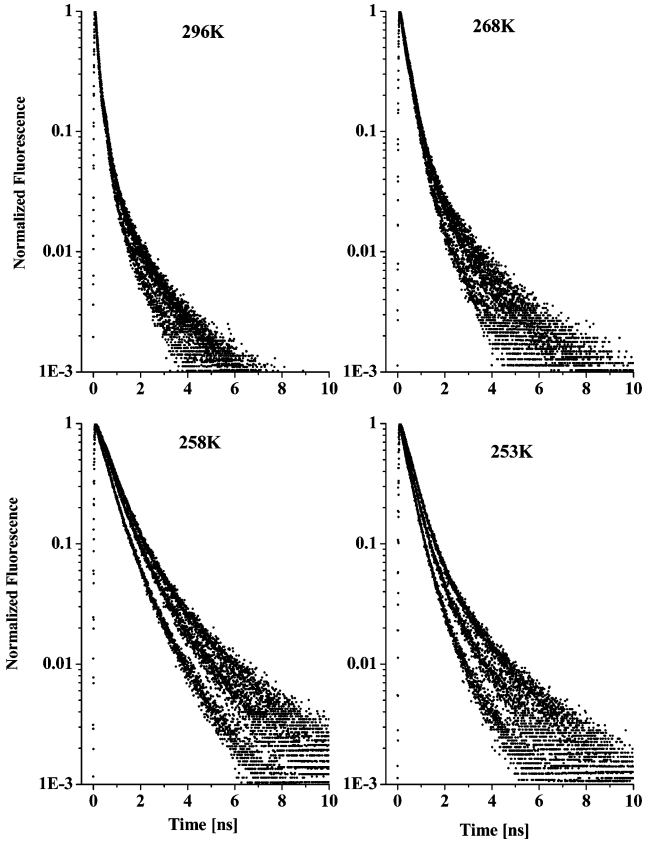

Figure 2. Time-resolved emission of the HPTS ROH band in pure water and in aqueous solution containing 4 and 18 mM of $NaNO_3$.

as the temperature decreases. The relative fluorescence of the ROH band is given approximately by

$$\frac{\Phi(T)}{\Phi_0} = \frac{k_0}{k_{PT}(T) + k_0} \tag{8}$$

The relative fluorescence of the RO^-* when exciting the ground-state ROH is given by

$$\frac{\Phi'(T)}{\Phi'_0} = \frac{k_{PT}(T)}{k_{PT}(T) + k_0} \tag{9}$$

where k_0 is the radiative rate of ROH, Φ_0 is the fluorescence quantum yield of ROH in the absence of proton transfer. Φ and Φ' are the fluorescence quantum yields of the ROH and RO^- forms of the HPTS, repsectively. Φ'_0 is the fluorescence quantum yield of direct excitation of the RO^-. At room temperature $k_{PT} = 10\ ns^{-1}$, whereas $k_0 = 0.19\ ns^{-1}$ is temperature independent. As the temperature decreases, Φ/Φ_0 increases. At about 220 K $k_{PT} \sim k_0$ and the fluorescence intensity of ROH is about 0.5 that at very low temperatures $T < 100$ K where $k_{PT} \ll k_0$. The fluorescence intensity ratio between the ROH and RO^- bands Φ'/Φ is given by

$$\frac{\Phi'(T)}{\Phi(T)} = \frac{k_{PT}}{k_0}(T) \tag{10}$$

In salt solution, at a specific temperature, the ROH band intensity is smaller than that of the pure (salt free) solution. The reason for that is the effective screening by the salt ions of the attractive potential between the RO^- and the proton both in the liquid solution and in ice.

Time-Resolved Emission. Figure 2 shows, on a semilog scale, the time-resolved emission at several temperatures of the ROH band of HPTS measured at 437 nm in pure water and in aqueous solution containing 4 and 18 mM of $NaNO_3$. As the temperature decreases, the average decay times of the signals increases. The longer decay time is attributed to the substantial decrease in the proton-transfer rate in ice as the temperature decreases.

The time-resolved emission of the ROH* band is composed of two parts. At short time the decay is fast and nearly exponential. The longer time of the fluorescence is nonexponential and forms a long-time tail. The reversible geminate recombination model is successfully used to fit this complex decay pattern. In general, the short time component is attributed to the rate of proton transfer, whereas the long-time nonexponential fluorescence tail is attributed to the reversible geminate recombination of the proton with RO^-. In the decay profiles of ROH in the presence of inert salt ions the amplitude of the long-time decay component is reduced at all temperatures. The geminate recombination reaction of a proton with an RO^- anion is assisted by diffusion in both the liquid and the solid phase. The Coulomb attraction enhances the probability to recombine geminately. The salt ions screen the Coulomb potential and decrease the attraction of the proton with RO^- after it is transferred from the photoacid to liquid water. The important point to note is that this reaction also occurs in the ice and inert salt strongly reduces the amplitude of the long-time fluorescence tail. As seen in Figure 2, in salt solution the intensity of the long-time nonexponential fluorescence tail is strongly reduced, in ice solution, at all temperatures, indicating that the Coulomb potential screening in ice is much larger than in the liquid phase. At about 10 mM the average salt ion distance is about 55 Å. In hexagonal ice structure this distance is equivalent to about 18 water molecules. The screening of the proton$-RO^-$ potential is easily observed as a reduction in the intensity of the long-time tail of the time-resolved emission of the phatoacid ROH* form.

Figure 3 shows the time-resolved emission of the RO^- band measured at 520 nm for an aqueous solution at several temperatures. The RO^- signal has a distinctive buildup time (rise time) that is followed by an exponential decay of about 5.2 ns. The rise time of RO^- emission is attributed to the rate of proton transfer. The longer the rise time of RO^- the slower the proton-transfer rate. As the temperature decreases, the rate constant, k_{PT}, is smaller and the rise time of RO^- gets longer. At a very low temperature $T < 220$ K the proton-transfer rate constant k_{PT} is smaller than the radiative rate of ROH, $k_{PT} < k_0$. At this low-temperature region the ratio of the ROH and RO^- fluorescence quantum efficiencies $\Phi'/\Phi \ll 1$. The overlap between the ROH and RO^- band shape function at about 515 nm, the RO^- peak position, is about 15%. The signal measured at 515 nm is a superposition of a strong ROH and a small RO^- fluorescence band (see Figure 1). The ROH time-resolved signal has an immediate rise time whereas the RO^- has a slow distinct rise time. Therefore, at a sufficiently low temperature the rise time of the total signal measured at about 515 nm exhibits a relatively faster rise time than at higher temperatures. The steady-state emission at low temperature supports this explanation.

Figure 4 shows, for several temperatures, the time-resolved emission of the ROH band of 2-naphtol-6,8-disulfonate (2N68DS), measured at 375 nm in two solutions: a pure aqueous solution that did not contain salt ions and a solution that contained 22 mM NaCl. As in the case of HPTS (the time-resolved fluorescence signals of the ROH in salt solution), the amplitude of the long-time nonexponential fluorescence tail slightly reduces in the liquid phase whereas it strongly reduces in the

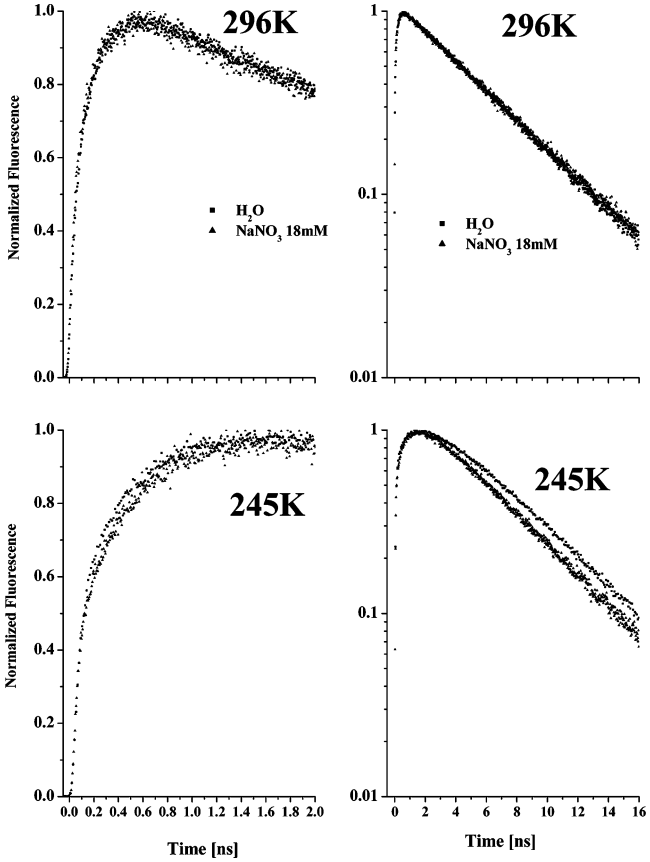

Figure 3. Time-resolved emission of the RO^- band of an aqueous solution and a solution containing 18 mM $NaNO_3$.

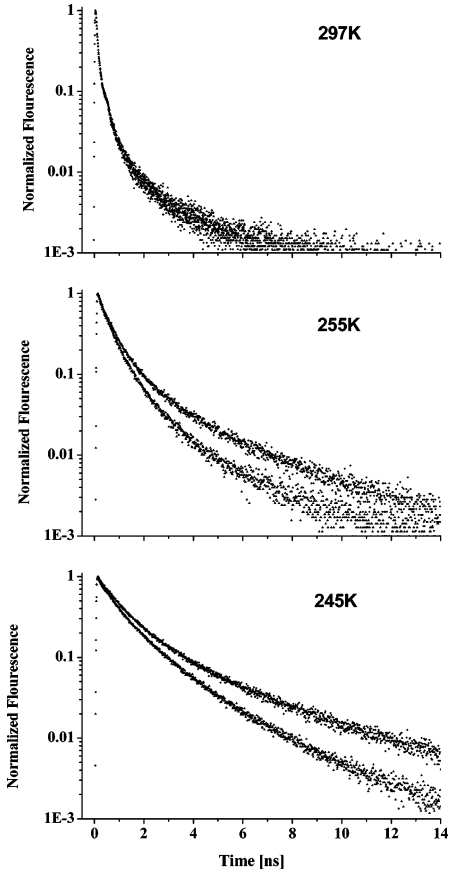

Figure 4. Time-resolved emission of the ROH band 2N68DS in aqueous solution and 22 mM NaCl solution, upper curves-pure water.

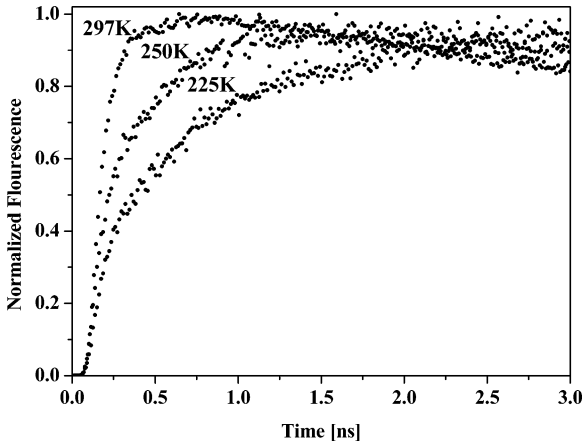

Figure 5. Time-resolved emission of 2N68DS of the RO^- band in aqueous solution at several temperatures.

ice phase. The inert salt ions in ice effectively screen the Coulomb attraction between the protons and the RO^- and thus the probability of geminate recombination to re-form the ROH* is strongly reduced.

Figure 5 shows the time-resolved emission of the RO^- of 2N68DS measured at 475 nm, slightly to the red of the RO^- peak (470 nm). The signal exhibits a distinctive rise time followed by an exponential decay with a decay time of about 12 ns. The rise time increases as the temperature decreases. Using the geminate recombination model, the signal of the RO^- can be fitted with the same parameters that are used to fit the complex decay profile of the ROH form of 2N68DS.

GR Model Fitting Procedure and Treatment of the Adjustable Parameters. k_{PT} determines the initial slope of the decay curves: the larger k_{PT}, the faster the initial exponential drop. The intrinsic recombination rate constant, k_r, hardly affects the behavior at $t \rightarrow 0$ but determines the magnitude of the long-time tail. The effect of increasing k_r is somewhat similar to decreasing D. It differs from the effect of changing R_D or a on the curvature of these plots. The parameters for the numerical solution of the DSE were taken from the literature.[30,34] The contact radius $a = 6$ Å is slightly larger than the molecule's spherical gyration radius (4.5−5.5 Å), obtained from measurements of HPTS rotation times.[35] It probably accounts for at least one layer of water molecules around the HPTS anion. All the abovementioned parameters, except the contact radius a, are temperature dependent. The temperature dependence of $D(T)$ and $\epsilon_s(T)$ of pure water in the liquid and supercooled liquid are given in the literature.[36−40]

At room temperature and neat water there are only two free adjustable parameters in solving and fitting the experimental data, the proton-transfer rate k_{PT} and the recombination rate k_r. The literature only covers the proton conductance in the liquid phase as a function of temperature in neat water solution. The values of proton diffusion in ice were measured in the seventies by Kelly and Salmon[19] and Camplin and Glen.[41] It was found that D_{H^+} is smaller by about a factor of 2 than in the liquid at about 268 K, 5 deg below the freezing point, $D_{H_+}^{ice} \sim 3.5 \times 10^{-5}$ cm^2/s. At the intermediate times, between the initial nearly exponential decay and the asymptotic $t^{-3/2}$ power law (0.1 ns $< t <$ 1 ns in pure water), k_r is the dominant parameter that determines the quality of the fit. The diffusion constant mainly affects the long-time fluorescence amplitude ($t >$ 1 ns in pure water). We used a value $D = 3.5 \times 10^{-5}$ cm^2/s in ice at the freezing point to obtain the best fit. We decreased the values $D(T)$ with the temperature decrease. The value of $\epsilon_s(T)$ in ice

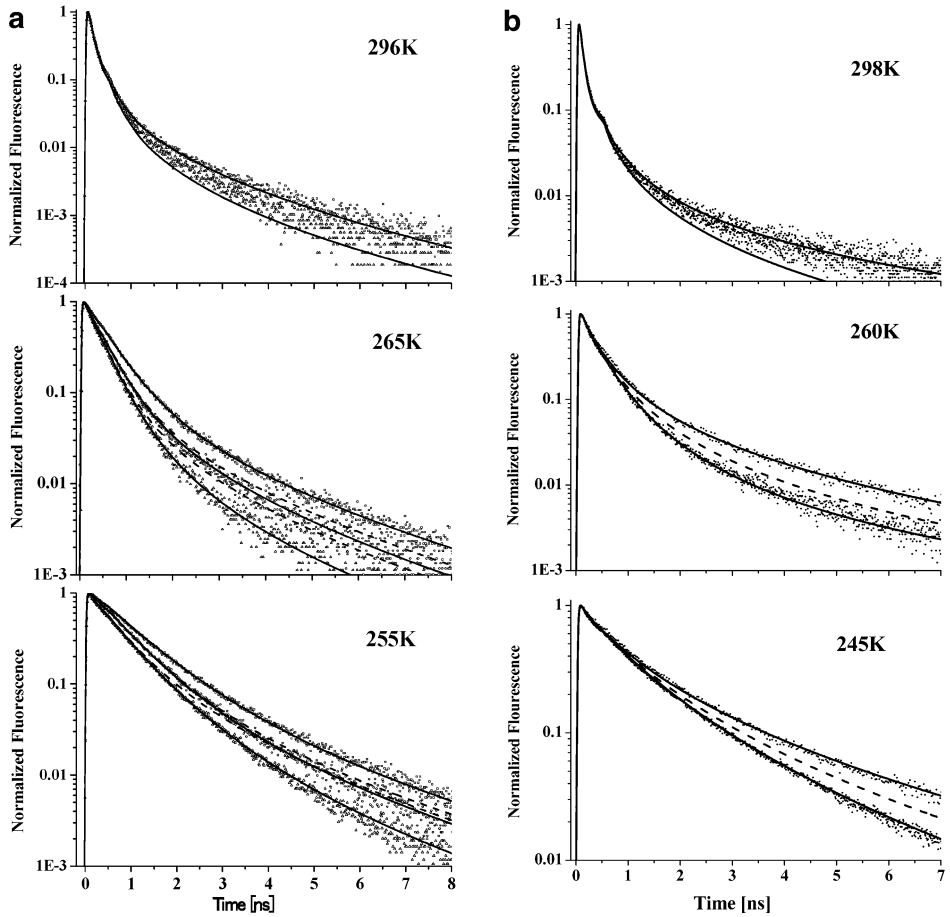

Figure 6. Time-resolved emission of ROH* in pure water solution and in solutions containing inert salt (symbols) along with a computer fit using the GR model: (solid line) calculation with effective concentration; (broken line) calculation based on the real concentration; (upper curve) pure water; (lower curve) salt solution. (a) HPTS in 18 mM $NaNO_3$ solution. (b) 2N68DS in 11 mM NaCl solution.

increases almost linearly with the temperature decrease. The expressions of both R_D and κ_{DH}^2 contain in the denominator $\epsilon_s T$. In ice the term $\epsilon_s T$ is almost temperature independent, and therefore both R_D and κ_{DH} are almost constant at all temperatures.

To summarize: When D_{H^+} is known from independent measurements (conductance), the two free fitting parameters are k_{PT} and k_r. In most of the experimental data represented in this study, $D_{H^+}(T)$ is unknown and thus D_{H^+} is an additional adjustable parameter that we chose by best fit and the knowledge of its values in similar systems or at other temperatures. In general, if $k_{PT} > k_r$ and D is small, $D \leq 10^{-5}$ cm^2/s then the value of k_{PT} mainly controls the initial decay of ROH at short times. Once k_{PT} is approximately determined k_r, and D control the amplitude of the longer times. k_r strongly affects the shape and amplitude of the intermediate times $1/k_{PT} < t < 3/k_r$. Once k_r is determined, D is the only parameter left to control the amplitude of the long times of the emission curve of the ROH.

Quantitative Analysis of the Proton Reaction in the Presence of an Inert Salt. Figure 6a shows the time-resolved emission of ROH* of HPTS in pure water solution and in solutions containing inert salt along with a computer fit using the GR model.

As seen in the figure, in the case of the salt solutions, the long-time fluorescence tail intensity is strongly reduced. In the fitting procedure of the luminescence curves of the salt solution we calculated the Coulomb potential screening by the Debye−Hückel expression given by eq 4. Two important points to note: (1) The experimental salt effect in ice is larger than the calculated. To fit the salt solution data, we used an effective value for the concentration rather than the real homogeneous concentration. In the discussion section we devote a lengthy explanation for plausible reason for the observed large salt effect. The second important point to note is that we used the values of the fitting parameters k_{PT}, k_r and D_{H^+} of the pure water solution data to fit the fluorescence curves of the salt solution. The values of k_{PT}, k_r, D_{H^+} used to fit the time-resolved fluorescence of HPTS in salt solution are given in Table 1. When the temperatures of the measurements of the two samples were not identical, we used an interpolation procedure to deduce a set of the parameters. The computer fits shown as solid lines are rather good at all temperatures above $T > 240$ K.

TABLE 1: Fitting Parameters of the Screened Potential Geminate Recombination Model for HPTS in 4 mM $NaNO_3$ Solution

T [K]	$k_{PT}{}^a$ [10^9 s^{-1}]	$k_r{}^{a,b}$ [10^9 Å s^{-1}]	D^c [cm^2 s^{-1}]	A^d
296	8.8	4.5	1.0×10^{-4}	
268	3.5	2.3	4.0×10^{-4}	2.89
265	2.8	2.2	$3.5 \times 10^{-4}{}^c$	3.24
263	2.3	1.8	3.0×10^{-5}	3.61
260	1.9	1.6	2.5×10^{-5}	3.61
258	1.5	1.4	2.2×10^{-5}	3.61
255	1.3	1.3	2.0×10^{-5}	3.61
253	1.1	1.2	1.9×10^{-5}	1.69
250	1.0	1.2	1.8×10^{-5}	1.0

[a] k_{PT} and k_r are obtained from the fit of the experimental data by the GR model (see text). $\tau_{ROH}{}^{-1} = 0.18$ ns^{-1}, $\tau_{RO}{}^{-1} = 0.19$ ns^{-1}. [b] The error in the determination of k_r is 50%; see text. [c] Free adjustable parameter. [d] Best fit correction factor of the salt concentration, $c' = Ac_{salt}$; see text.

TABLE 2: Fitting Parameters of the Screened Potential Geminate Recombination Model for 2N68DS in 22 mM NaCl Solution

T [K]	k_{PT}[a] [10^9 s^{-1}]	k_r[a,b] [10^9 Å s^{-1}]	D[c] [cm^2 s^{-1}]	A[d]
298	12	10	1.0×10^{-4}	4
268	6.2	8.5	4.5×10^{-5}	4
263	5	7.5	4.0×10^{-5}	4
260	4	7	3.0×10^{-5}	4
255	2.2	4	1.8×10^{-5}	4
253	2	4	1.7×10^{-5}	4
248	1.5	3.8	1.6×10^{-5}	4
245	1.4	3.7	1.6×10^{-5}	4

[a] k_{PT} and k_r are obtained from the fit of the experimental data by the GR model (see text). $\tau_{ROH}^{-1} = 0.11$ ns^{-1}, $\tau_{RO^-}{}^{-1} = 0.083$ ns^{-1}. [b] The error in the determination of k_r is 50%; see text. [c] Free adjustable parameter. [d] Best fit correction factor of the salt concentration, $c' = Ac_{salt}$; see text.

It is encouraging to note the success of the geminate recombination model to fit the salt samples with the same k_{PT}, k_r and D_{H^+} parameters of the salt-free solution. At a low enough temperature the proton-transfer reaction is slow and comparable with the radiative rate $k_0 = 0.19$ ns^{-1} ($\tau_r = 5.2$ ns). In such a case the long-time fluorescence tail of the geminate recombination process merges with the fast decay phase attributed to the proton-transfer process. The overall decay profile is nearly exponential. At such a low temperature the effect of salt ions on the luminescence of ROH is small. Thus there is a low-temperature limit in which the Coulumb potential screening effect can be observed. We estimate that below 240 K the screening effect cannot be followed quantitatively by the geminate recombination model. Figure 6b shows the time-resolved emission of ROH* of 2N68DS in pure water solution and in solution containing inert salt along with a computer fit using the GR model. We used the same procedure in the fit of data as described for HPTS. The fitting parameters are given in Table 2.

Analysis of the Steady-State Spectrum. The steady-state emission of HPTS at various temperatures is shown in Figure 1. At low enough temperature $T < 150$ K where $k_0 > k_{PT}$ the emission spectrum is only that of the protonated form. The emission band shows a distinctive vibronic structure with a progression of about 1100 cm^{-1}. We fit the structured emission spectrum by assigning a log-normal line shape function to each vibration band.[42] To obtain a good fit to the ROH emission band, we used four vibration bands. The two high-energy bands are of about equal intensity, whereas the relative amplitude of the subsequent two lower energy bands is smaller and has decreasing amplitude with decreasing energy. This type of spectrum is a consequence of the Franck−Condon principle. When the ground and first electronically excited potential surface are displaced with respect to a generalized coordinate, the relative amplitude of the vibration progression is given by the Huang−Rhys factor S_0. The relative amplitude of each individual vibration peak is given by $S_o^n/n!$, where n is a number in the sequence of the vibration levels in the spectrum. When $S_0 \approx 1$, then the intensity of the second vibration band is of about the same intensity of the first one and the intensity of the subsequent vibration bands decreases monotonically. From the band analysis of the emission spectrum of the ROH band at low temperature the relative intensities of the four vibrations fits approximately to the case $S_0 \simeq 1$.

The ROH emission band shifts to the red as the temperature increases. The 0−0 band shifts from about 23 400 cm^{-1} at about 100 K to about 22 900 cm^{-1} at 220 K. At higher temperatures the analysis of the band structure gets difficult because the ROH band intensity decreases sharply because of the efficient excited-state proton-transfer process when $k_{PT} > k_0$. The bandwidth of each vibration band increases with the temperature increase. At about 100 K the bandwidth is around 1250 cm^{-1} whereas at 220 K it is about 1750 cm^{-1}. We find a one to one correspondence between the Stokes shift of the emission band and the vibration bandwidth. This type of relation is expected from the fluctuation dissipation theory of Kubo.[43]

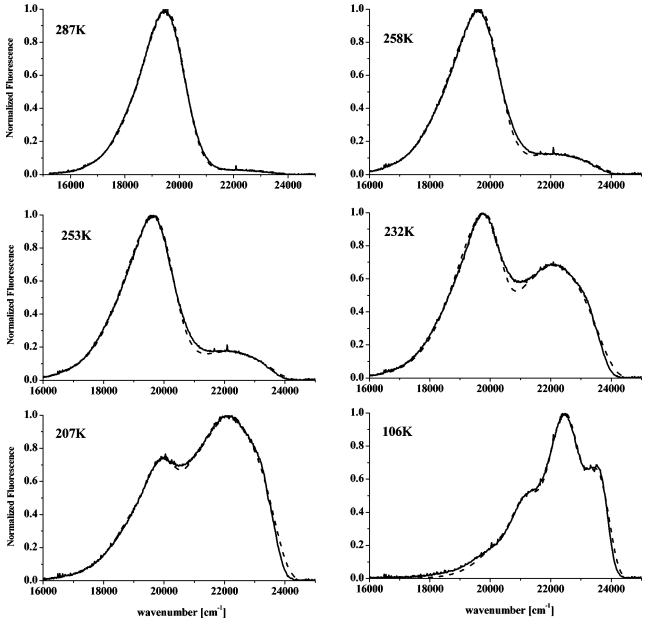

Figure 7. Experimental (solid line) and a fit, (broken line) of the steady-state spectra of HPTS in pure water solution.

The intensity of the RO$^-$ band at high temperatures $T >$ 240 K is larger than the ROH band intensity. Its position and bandwidth is only slightly dependent on the temperature. Equations 8−10 roughly provide the intensity of each band and the ratio between them. We quantitatively fit the RO$^-$ band with two lognormal bands the high-energy band is nearly Gaussian with a peak at about 19 500 cm^{-1} and a width of 1500 cm^{-1}. The low-energy band intensity is smaller by about a factor of 5. It is positioned at about 18 500 cm^{-1} and is highly asymmetric. Figure 7 shows the experimental and a fit of the steady-state spectra of HPTS in pure water solution at several temperatures. At a particular temperature the shape of the ROH and RO$^-$ bands is the same for pure water sample and in the presence of an inert salt. At temperatures above 220 K the intensity of ROH band of the salt solution is smaller than the intensity of the ROH band of the pure water solution. This is explained by the screening of the Coulomb potential by the salt ions and as a consequence it decreases the proton-RO$^-$ geminate recombination probability to reform back the ROH population. The emission intensity depends on the time integrated ROH population, which is smaller in the salt solution.

Figure 8 shows a plot of the logarithm of $(\Phi'/\Phi)k_0$ as a function of $1/T$ along with an additional plot of the values of log k_{PT} extracted from the time-resolved analysis versus $1/T$. $(\Phi'/\Phi)k_0$ provides on estimate for k_{PT} and ignores the geminate recombination contribution to the fluorescence of ROH and RO$^-$. As seen from the figure at high energy, both plots show approximately an Arrhenius behavior. The plot of log k_{PT} versus $1/T$ is more accurate than that of $(\Phi'/\Phi)k_0$ at high temperatures where k_{PT} is determined from the quantitative analysis of the ROH decay curve by the GR model. At temperature below $T <$ 240 K, the rate constant of proton transfer, k_{PT}, is small, the head and tail of the ROH curve coalesce, and the decay rate of

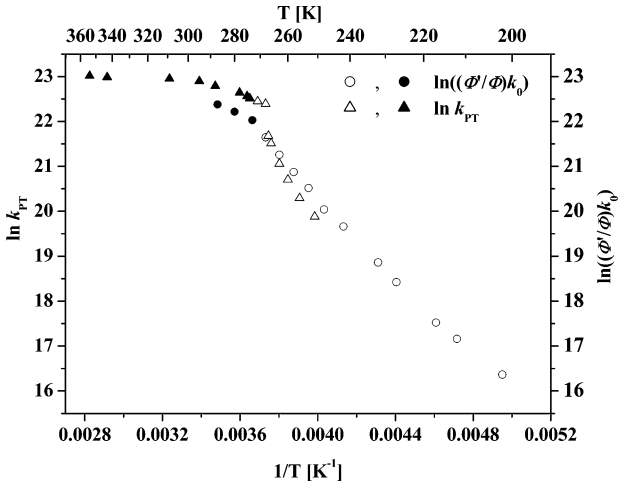

Figure 8. Arrherenius plot of the logarithm of $(\Phi'/\Phi)k_0$ and log k_{PT} as a function of $1/T$: (full symbols) liquid; (open symbols) ice.

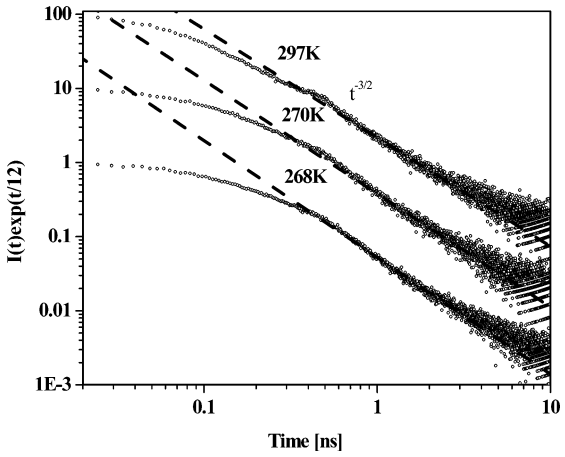

Figure 9. log−log plot of I_{ROH} exp(t/τ_f) for 2N68DS at several temperatures in water solution containing 22 mM NaCl. The individual curves are shifted vertically for clarity purpose.

the ROH fluorescence is mainly determined by k_0, the radiative rate constant. In such a case the time-resolved emission cannot accurately provide the value of k_{PT}, whereas the steady-state emission analysis provides a better estimate for k_{PT} at lower temperatures.

Discussion

In previous papers on proton transfer in ice we published data only at high temperatures above 220 K. In this contribution we extend our measurement to lower temperature, $T \sim 90$ K. In previous studies in ice we used only a single photoacid, the HPTS. In this study, we measured the proton transfer and geminate recombination rates of HPTS and 2N68DS as a function of temperature, in liquid water and ice containing a small amount (<30 mM) of an inert salt like sodium chloride and sodium nitrate.

In general, both photoacid results provide the same information on the effective screening of electrolytes in ice. The main finding in the current study is that the screening salt effect in ice is much larger than that in the liquid state. We explain the large screening in ice by the "salting-out" effect in ice that concentrates the impurities to confined volumes to minimize the ice crystal energy.

Effect of Methanol on the Photoprotolytic Cycle in Ice. In the experiments described in this paper there is a difficulty in describing the microscopic ice structure surrounding the photoacid. The ice we prepare contains three impurities, the large photoacid molecule, the inert salt ions and methanol. The largest amount of impurities is the methanol we added to the water. In pure ice we find that the emission of the photoacid is reduced by orders of magnitude when the liquid sample freezes. Addition of a small amount of protic solvent like alcohols to water is essential in these experiments to prevent "sating out" of the photoacid from the ice. In most of the experiments we used a methanol concentration of about 0.5 M. Thus a 1:100 molar ratio between methanol and water. In liquid water at 298 K such an amount of methanol reduced the rate constants k_{PT} and k_r of the photopritolytic cycle by about 5%. In several experiments we qualitatively checked the effect of further reducing the methanol concentration on the photoprotolytic cycle. In these experiment we were able to prevent the "salting-out" of the photoacid at a methanol concentration of about 50 mM, 10-fold less than in most of the experiment. We found in water/methanol mixture of only 50 mM methanol that the time-resolved emission is almost unaffected by the large change in the methanol concentration. The analysis of the experimental results of a sample that contained only 50 mM of methanol shows that the main parameters of the geminate recombination model: k_{PT}, k_r, D_{H^+} as well as the inert salt screening effect are about the same as for 10 fold methanol concentration (0.5 M).

The few methanol molecules next to the photoacid are probably positioned close to the hydrophobic part of the photoacid structure. The methanol CH_3 group is close to the center of the photoacid aromatic ring (hydrophobic interaction). The OH group of the methanol is pointing toward a water molecule in the ice. The average distance between the inert salt ions of a 10 mM solution is about 55 Å. This distance is equivalent to a distance of 20 water molecules in the ice structure. On the basis of the proton diffusion constant in ice, the diffusing proton is also visiting ice structure sites that are far removed from the photoacid, and their structure is close to hexagonal. The overall number of water molecules in the volume around the photoacid that the proton may visit within a 10 ns window is about 32 000. In the 50 mM methanol ice sample the number of dopants including the salt ions is only about 30.

From the steady-state spectra (see Figures 1 and 7) we find that inert salt ions do not tend to change the shape of the ROH and RO^- spectra. This indicates that the ions at concentrations <30 mM do not form complexes with the photoacid. This implies that the ions are at least one water molecule apart from the photoacid. Our assumption that the inert salt ions form an ionic atmosphere surrounding the ROH molecule is reasonable. Upon water freezing, those ions tend to keep their positions around the ROH. This ion arrangement in ice screens the Coulomb potential in the vicinity of the photoacid.

Justification for a Proton Diffusion Formalism in Ice. The theory of the diffusion assisted reversible geminate recombination model describing the photoprotolytic cycle of a photoacid shows that under a quasi-equilibrium condition (several photocycles of proton transfer and geminate recombination) the time-resolved fluorescence of ROH* multiplied by the excited-state life time obeys at long times a power-law decay (see eq 6). For three dimensions, it assumes the power law of $t^{-3/2}$. Figure 9 shows a log−log plot of $I(t)_{ROH}$ exp(t/τ_f) for 2N68DS at several temperatures in water in the presence of 22 mM NaCl. As seen in the figure, the long-time fluorescence tail indeed shows a decay of a power law (straight line) with a slope of about 1.5 ± 0.2 for both pure water and salt solution at a large temperature range.

Using the values $D = 4 \times 10^{-5}$ cm^2/s for proton diffusion in ice at 268 K and the long time of the time resolve measurements

of about 10 ns, we can estimate the proton diffusion length ($L \simeq \sqrt{Dt} \approx 65$ Å).

In numerous experiments in the past decade we found in liquid water that indeed a power law exists and it is a good criteria for the diffusion model. There is a possibility that the proton motion in ice can proceed via a very long distance jump, so-called Grothus mechanism. Our experiments cannot identify the nature of the mechanism of proton movement in ice. It is accustomed to use the theory of Jaccard[44] to explain[15,16] the electrical properties of ice, namely, the electrical conductivity of ice[41] and its dielectric properties measured by Steinman.[45]

According to Jaccard theory[44] the electrical properties of ice are largely due to two types of defect within the crystal structure that allow protons to move along the hydrogen bonds under the influence of an external field. Ion defects are produced when a proton moves from one end of the bond to the other, thus creating a H_3O^+, OH^- ion pair. Conduction is then possible by means of successive proton jumps. Bjerrum defects are orientational defects caused by the rotation of a water molecule to produce either a doubly occupied bond (D-defect) or a bond with no protons (L-defect). A series of successive rotations will produce conduction, and neither process alone can explain the dc conduction. For example, the movement of a H_3O^+ ion sets the protons in such a position that no more H_3O^+ ions may subsequently follow the same path. A similar effect occurs with Bjerrum defects. However, if an ion defect is followed by a Bjerrum defect, then the protons will be reset into their original positions and the conduction pathway unblocked.

We used the diffusion assisted geminate proton$-RO^-$ recombination model (GR model) to quantitatively fit the time-resolved emission of the photoacid embedded in the frozen matrix of ice, including the inert salt ions, as impurities. The GR model predicts that the long-time fluorescence tail of ROH band multiplied by the excited-state lifetime (see eq 6) will decay at long times as a power law of $t^{-3/2}$. The power law is also predicted for liquid and solid water solution with inert salt that partially screens the Coulomb potential between the proton and the RO^-. The long-time asymptotic expression, given in eq 6, shows that the salt effect reduces the term $\exp[V(a)]$ but does not affect the power low of $t^{-3/2}$. $V(r)$ is given by eq 3 using the Debye−Hückel screening potential. Extrapolating $V(a)$ from eq 4 gives

$$V(a) = \left[\frac{1}{1 + \kappa_{DH} a}\right] \tag{11}$$

For 10 mM of inert salt at 250 K $< T <$ 300 K, $\epsilon_s^{ice} \cong 100$, $\epsilon_s^{liquid} \cong 80$, $a = 6$ Å, $\kappa_{DH} a \simeq 0.2$, the asymptotic fluorescence tail should reduce by about 15%. Figure 6a shows the time-resolved emission of ROH of HPTS and the quantitative fit in pure water solution and in 18 mM $NaNO_3$ solution in the liquid and ice. The fit using the exact salt concentration is given by the broken line and the solid line is the best fit by the GR model when the salt concentration is a free adjustable parameter. In the liquid phase at 298 K the screened Debye−Hückel potential overestimates the salt effect on the ROH time-resolved emission. This was also found in our previous study.[26] In the solid ice phase we find the opposite, the Debye−Hückel screened potential underestimates the actual experimental salt effect on the ROH time-resolved emission (broken line). To get a better fit of the calculated curve, we used the salt concentration as a free adjustable parameter. In the ice at the temperature range 255 K $< T <$ 270 K the effective salt concentration c' is about a factor of 4 larger than the actual salt concentration, $c' = 4c_{salt}$. At a temperature lower than $T \leq 250$ K the effective concentration slightly decreases with the temperature decrease. At $T =$ 250 K the effective concentration is about 2.5 larger than the actual concentration; see Table 1.

We also studied the salt effect on the luminescence of 2-naphthol-6,8-disulfonate (2N68DS). The 2N68DS ROH is negatively charged, $z = -2$ compared to $z = -3$ for HPTS. The experimental time-resolved emission of the ROH form of 2N68DS in liquid water salt solution of 22 mM $NaNO_3$ or 11 mM NaCl shows a very small salt effect. The calculations based on Debye−Hückel screened potential overestimate the small experimental salt effect in the liquid phase at high temperature $T \sim 300$ K. In ice we find that the time-resolved emission of ROH 2N68DS cannot be quantitatively fitted with Debye−Hückel screened Coulomb potential with the correct salt concentration. As in the case of HPTS, we get a rather good fit in ice by the GR model with screened Debye Hückel potential using an effective concentration of about a factor of 4; see Figure 6b. The fitting parameters for 2N68DS including the correction factor for the salt concentration are given in Table 2.

The question arises why the experimental salt effect of both HPTS and 2N68DS in ice strongly deviated from the calculated curves that underestimate the large salt effect. A plausible reason is given along the lines of the well-known salting-out effect upon freezing of a salt solution. On a microscopic level the nature of the local environment next to the two photoacids in ice is different from that in the liquid water. In ice the impurities tend to be confined in small volumes to minimize the ice crystal energy. In ice the local environment next to a photoacid molecule contains salt concentration larger than the homogeneous concentration, c_0.

An alternative speculative explanation for the large salt effect in ice concerns the possible increase of the dielectric constant next to the photoacid. The parameters given in eq 6 that govern the intensity of the long-time fluorescence tail are D, $\exp[V(a)]$, k_r and k_{PT}. In general, it is difficult to differentiate between the different parameters, except k_{PT}, which is determined from the initial decay rate of the contribution of ROH time-resolved emission. The amplitude of the long-time fluorescence tail decreases if $V(a)$ decreases. The Debye radius R_D (eq 3) depends on $1/\epsilon_s$ and the screening potential parameter κ_{DH} depends on $1/\sqrt{\epsilon_s}$. If the dielectric constant in doped ice increases with salt concentration, then the long-time tail intensity should also decrease as a consequence of the increase in the dielectric constant with the salt concentration.

According to Jaccard theory[44] the value of the dielectric constant strongly depends on the imperfection of the ice structure. In ice there are four types of defects, two orientational defects D and L and two inonizing defects OH^- and H^+. According to the theory the dielectric constant difference, $\epsilon_s - \epsilon_\infty$ (where ϵ_∞ is the high-frequency value) strongly depends on the difference in the population between the two kinds of defects[15] (eq 9.34 in ref 15). In the equation numerator the contribution to the dielectric constant of the population density of the DL defects and that of the ionizing defects have opposite signs and thus can cancel each other. Steinmann[45] has measured the dielectric properties of ice doped with hydrogen fluoride. It was found that the dielectric constant of doped ice decreases to about the high-frequency dielectric constant ϵ_∞ as the concentration increases. It is possible that inert salt, like NaCl and $NaNO_3$, changes the densities of the defects in ice in such a way that the effective dielectric constant increases and thus the Coulomb potential decreases and the fluorescence long-time tail decreases.

Summary

In this contribution we studied the salt effect on the excited-state proton transfer in ice. Time-resolved emission was employed to measure the photoprotolytic cycle of excited photoacid as a function of temperature, in liquid water and in ice, in the presence of an inert salt.

As was found previously in the liquid phase, the proton is first transferred from the photoacid to a nearby water molecule. Subsequently, it diffuses in the ice under the influence of the Coulomb potential between H^+-RO^- that enhances the geminate recombination. In the presence of an inert salt the Coulomb potential is partially screened by immobile inert salt ions in the ice phase. We used two photoacids, HPTS and 2-naphtol-6,8-disulfonate (2N68DS) and two inert salts, $NaNO_3$ and NaCl. 2N68DS ($pK^* \sim 0.7$) is a stronger photoacid than HPTS ($pK^* \sim 1.35$) and transfers a proton to liquid water at about 40 ps. In general, both photoacid results provide the same information on the effective screening of electrolytes in ice.

We used the Debye−Hückel theory to express the screening of the Coulomb electrical potential by the inert salt. We find that in the liquid phase the measured screening effect is small and the Debye−Hückel expression slightly overestimates the experimental effect. In ice, the screening effect is rather large and the Debye−Hückel expression underestimates the measured effect. We explain the large screening in ice by the "salting-out" effect in ice that tends to concentrate the impurities to confined volumes to minimize the ice crystal energy.

Acknowledgment. We thank Prof. N. Agmon and Prof. M. Gutman for their helpful and fruitful suggestions and discussions. This work was supported by grants from the Binational US-Israel Science Foundation, the James-Franck German-Israel Program in Laser-Matter Interaction.

References and Notes

(1) Bell, R. P. *The Proton in Chemistry*, 2nd ed.; Chapman and Hall: London, 1973.
(2) *Proton Transfer Reaction*; Caldin, E. F., Gold, V., Eds.; Chapman and Hall: London, 1975.
(3) (a) Weller, A. *Prog. React. Kinet.* **1961**, *1*, 189. (b) *Z. Phys. Chem. N. F.* **1958**, *17*, 224.
(4) (a) Eigen, M. *Angew. Chem., Int. Ed.* **1964**, *3*, 1. (b) Eigen, M.; Kruse, W.; Maass, G.; De Maeyer, L. *Prog. React. Kinet.* **1964**, *2*, 285.
(5) Ireland, J. E.; Wyatt, P. A. *Adv. Phys. Org. Chem.* **1976**, *12*, 131.
(6) (a) Gutman, M.; Nachliel, E. *Biochem. Biophys. Acta* **1990**, *391*, 1015. (b) Pines, E.; Huppert, D. *J. Phys. Chem.* **1983**, *87*, 4471.
(7) Kosower, E. M.; Huppert, D. *Annu. Rev. Phys. Chem.* **1986**, *37*, 127.
(8) Tolbert, L. M.; Solntsev, K. M. *Acc. Chem. Res.* **2002**, *35*, 1.
(9) (a) Rini, M.; Magnes, B. Z.; Pines, E.; Nibbering, E. T. J. *Science* **2003**, *301*, 349. (b) Mohammed, O. F.; Pines, D.; Dreyer, J.; Pines, E.; Nibbering, E. T. J. *Science* **2005**, *310*, 5745.
(10) Prayer, C.; Gustavsson, T.; Tarn-Thi, T. H. In *Fast Elementary Processes in Chemical and Biological Systems*; 54th International Meeting of Physical Chemistry; AIP: New York, 1996; p 333.
(11) Tran-Thi, T. H.; Gustavsson, T.; Prayer, C.; Pommeret, S.; Hynes, J. T. *Chem. Phys. Lett.* **2000**, *329*, 421.
(12) Agmon, N. *J. Phys. Chem. A* **2005**, *109*, 13.
(13) Uras-Aytemiz, N.; Joyce, C.; Devlin, J. P. *J. Phys. Chem. A* **2001**, *105*, 10497.
(14) Devlin, J. P.; Gulluru, D. B.; Buch, V. *J. Phys. Chem. B* **2005**, *109*, 3392.
(15) Fletcher, N. H. In *The Chemical Physics and of Ice*; Cambridge University Press: Cambridge, U.K., 1970; Chapter 9.
(16) Hobbs, P. V. In *Ice Physics*; Clarendon Press: Oxford, U.K., 1974; Chapter 2.
(17) Petrenko, V. F.; Whitworth, R. W. *Physics of ice*; Oxford University: Oxford, U.K., 1999.
(18) Von Hippel, A.; Runck, A. H.; Westphal, W. B. In *Physics and Chemistry of Ice*; Walley, E., Jones, S. J., Gold, L. W., Eds.; Royal Society of Canada: Ottawa, 1973; p 236.
(19) Kelly, I. J.; Salomon, R. R. *J. Phys. Chem.* **1969**, *50*, 75.
(20) Smith, K. K; Huppert, D.; Gutman, M.; Kaufmann, K. *J. Chem. Phys. Lett.* **1979**, *64*, 22.
(21) Clark, J. H.; Shapiro, S. L.; Campillo, A. J.; Winn, K. J. *J. Am Chem. Soc.* **1979**, *101*, 746.
(22) Politi, M. J.; Fendler, J. H. *J. Am. Chem. Soc.* **1984**, *106*, 265.
(23) Pines, E.; Huppert, D. *J. Chem. Phys.* **1986**, *84*, 3576.
(24) Pines, E.; Huppert, D.; Agmon, N. *J. Chem. Phys.* **1988**, *88*, 5620.
(25) Goldberg, S. Y.; Pines, E.; Huppert, D. *Chem. Phys. Lett.* **1992**, *192*, 77.
(26) Pines, E.; Huppert, D.; Agmon, N. *J. Phys. Chem.* **1991**, *95*, 666.
(27) Agmon, N.; Goldberg, S. Y.; Huppert, D. *J. Mol. Liq.* **1995**, *64*, 161.
(28) Leiderman, P.; Gepshtein, R.; Uritski, A.; Genosar, L.; Huppert, D. *J. Phys. Chem. A* **2006**, *110*, 9039.
(29) Poles, E.; Cohen, B.; Huppert, D. *Isr. J. Chem.* **1999**, *39*, 347−360.
(30) Robinson, R. A.; Stokes R. H. *Electrolyte Solutions*, 2nd ed.; Butterworth: London, 1959; Appendices 1.1 and 6.2.
(31) Rice, S. A. In *Diffusion-Limited Reactions*; Computers in Chemistry and Kinetics, Vol. 25; Bamford, C. H., Tipper, C. F. H., Compton, R. G., Eds.; Elsevier: Amsterdam, 1985.
(32) Agmon, N. *J. Chem. Phys.* **1984**, *81*, 2811.
(33) Krissinel, E. B.; Agmon, N. *J. Comput. Chem* **1996**, *17*, 1085.
(34) Lewis, G. N.; Doody, T. C. *J. Am. Chem. Soc.* **1993**, *55*, 3504.
(35) Haar, H. P.; Klein, U. K. A.; Hfiner, F. W.; Hauster, M. *Chem. Phys. Lett.* **1977**, *49*, 416.
(36) Timmerman, J. *Physico-Chemical Constants of Binary Systems*; Interscience: New York, 1960; Vol. 4.
(37) Erdey-Gruz, T.; Lengyel, S. In *Modern Aspects of Electrochemistry*; Bockris, J. O'M., Conway, B. E., Eds.; Plenum: New York, 1964; Vol. 12, pp 1−40.
(38) Cornish, B. D.; Speedy, R. J. *J. Phys. Chem.* **1984**, *88*, 1888.
(39) Heise, V. R. Z. *Naturforsch.* **1958**, *13a*, 547.
(40) Erdey-Gruz, T.; Kugler, E. *Magy. Kem. Foly.* **1968**, *74*, 135 (in Hungarian).
(41) Camplin, G. C.; Glen, J. W. In *Physics and Chemistry of Ice*; Whalley, E., Jones, S. J., Gold, L. W., Eds.; Royal Society of Canada: Ottawa, 1973; p 256.
(42) Fraser, R. D. B.; Suzuki, E. In *Spectral Analysis*; Blackburn, J. A., Ed.; Marcel Dekker: New York, 1970; p 171.
(43) Kubo, R. *J. Phys. Soc. Jpn.* **1957**, *12*, 570.
(44) Jaccard, C. *Ann. N. Y. Acad. Sci.* **1965**, *125*, 390−400.
(45) Steinemann, A. *Helv. Phys. Acta* **1957**, *30*, 581−610.